REAL-TIME SIMULATION OF A DOUBLY-FED INDUCTION GENERATOR BASED WIND POWER SYSTEM ON eMEGASim® REAL-TIME DIGITAL SIMULATOR

By

Nasir Abdulai Boakye-Boateng

Approved:

Abdul R. Ofoli
Assistant Professor of Engineering
(Chair)

Ahmed H. Eltom
Professor of Engineering
(Committee Member)

Nurhidajat Sisworahardjo
Assistant Professor of Engineering
(Committee Member)

William H. Sutton
Dean of the College of Engineering and Computer Science

A. Jerald Ainsworth
Dean of the Graduate School

REAL-TIME SIMULATION OF A DOUBLY-FED INDUCTION GENERATOR BASED WIND POWER SYSTEM ON eMEGASim® REAL-TIME DIGITAL SIMULATOR

By

Nasir Abdulai Boakye-Boateng

A Thesis Submitted to the Faculty of the University
of Tennessee at Chattanooga in Partial
Fulfillment of the Requirements of the
Degree of Master of Engineering

The University of Tennessee at Chattanooga
Chattanooga, Tennessee

May 2013

ABSTRACT

The growing demand for wind power integration into the generation mix prompts the need to subject these systems to stringent performance requirements. This study sought to identify the required tools and procedures needed to perform real-time simulation studies of Doubly-Fed Induction Generator (DFIG) based wind generation systems as basis for performing more practical tests of reliability and performance for both grid-connected and islanded wind generation systems.

The author focused on developing a platform for wind generation studies and in addition, the author tested the performance of two DFIG models on the platform real-time simulation model; an average SimpowerSystems® DFIG wind turbine, and a detailed DFIG based wind turbine using ARTEMiS® components. The platform model implemented here consists of a high voltage transmission system with four integrated wind farm models consisting in total of 65 DFIG based wind turbines and it was developed and tested on OPAL-RT's eMEGASim® Real-Time Digital Simulator.

ACKNOWLEDGEMENTS

In the name of God, the Most Gracious, and the Ever Merciful: “Surely, there is ease after hardship”.

This work has been a testament not of my own efforts but of the many whose guidance and support has motivated the efforts of many that have culminated into this work. This acknowledgement is to especially highlight the most prominent among the many worthy of acknowledgement.

I am most appreciative of the committee Chairman Dr. Abdul R Ofoli, and members Dr. Ahmed Eltom and Dr. Nurhidajat Sisworahardjo for their guidance and their efforts to make available the necessary resources that made it possible to undertake this study.

I acknowledge the support of my family especially my daughter Nasira Boakye for being such an inspiration.

Thank you all.

TABLE OF CONTENTS

LIST OF FIGURES

CHAPTER I

INTRODUCTION

Background to the Study

Wind power generation has seen significant development over the past few years. This is due to increasing attraction to renewable energy sources motivated primarily by the concerns over CO_2 emissions and sustainability of conventional power generation; and the fact that wind power has emerged as clean, safe and economical [1-3]. Growing penetration of wind generation into power grids has come with several concerns including the impact of wind generators (WGs) on power system reliability, availability and power quality since these are highly dynamic generators of which the power industry has relatively limited experience [4-6]. Structurally, the conventional power transmission/distribution system is designed to deliver power from concentrated generation sources down to loads at the distribution level. WGs in distribution networks fundamentally invert this configuration by feeding power into the grid from sources located in the distribution networks and thus closer to the load [7]. This configuration, coupled with the dynamic nature of WGs makes it imperative that wind power generators provide ancillary services that promote reliability and performance. These include primary voltage regulation, primary power/frequency semi-regulation, power ramp capability and remote control of individual turbines [5].

The mechanical nature of wind energy has permitted the use of several types of WG such as fixed speed WG, limited variable speed WG, full-scale variable speed WG, and Doubly fed

Induction Generator (DFIG) based WGs [4]. However, the variable nature of wind speed makes variable speed constant frequency (VSCF) wind generation systems preferable over traditional constant speed constant frequency (CSCF) systems due to their better power capture, less mechanical stress, and lower power fluctuation. Three main VSCF wind power generator types are directly driven synchronous generators, squirrel cage induction generators and doubly fed induction generators (DFIGs) [8]. The DFIG based WG is dominating the market [9] because it has superior energy transfer efficiency, low investment and flexible control; a result of its ability to output a constant frequency AC, though the prime mover may operate at variable speed as in the case of WGs [10]. In addition, its four-quadrant active and reactive power capabilities permit independent control of active and reactive power or voltage, and proper regulation of mechanical stresses and acoustic noise in the Wind Turbine (WT) [2, 4, 7, 11].

Doubly-fed induction generator (DFIG) turbines are variable speed wind turbines that are able to operate at minimal heat loss by employing a back-to-back AC/DC/AC converter in the rotor circuit to recover the slip power. Real and reactive power outputs are decoupled through flux-vector control of rotor currents. This also leads to maximized wind power extraction and lowering of mechanical stresses. The stator side is directly connected to the grid and thus the converter only handles the power in the rotor circuit. The converter rating is therefore below the full machine rating since it is limited to only the rotor side power [2] [12].

In order to improve the performance and reliability of DFIG based WGs, several control schemes have been used to achieve a one or more objectives. For instance, in order to achieve Maximum Power Point Tracking (MPPT) schemes that included measuring or estimating of the wind speed [12] [13] use of mechanical output power feedback control [13] and the continuous search for the peak output power using the optimum algorithm [13-15] such as hill-climb

searching control strategy. These come with a myriad of challenges including the difficulty in estimating highly variable wind conditions, and the need for real-time measurement of wind conditions [16]. In addition, some fundamental drawbacks such as the failure to effectively factor in the efficiency of the DFIG in the design of these control schemes have been found to limit these control schemes. Further research has proposed schemes to address these challenges including controlling the generator stator active and reactive power since these depend both on the mechanical and electrical characteristics of the WG [8].

Significance of the Study

One limitation of most existing research is that propositions are tested in offline simulation environments only thus leaving a verifiability gap when it comes to practicality of the propositions [5, 9, 10, 11, 12]. Although a few authors have done real-time simulation of DFIG based wind power systems the scale has been relatively small [3]. This fact could be due to the limitation in the availability of real-time simulators and the proprietary nature of the techniques used in these simulators.

The author seeks to discuss the required tools and procedures needed to perform real-time simulations of DFIG based WG systems as basis for performing more practical testing of control strategies aimed at maximizing the reliability and performance of both grid-connected and islanded WG systems. This objective is achieved by discussing the simulation and testing of different wind farm configurations connected to a high voltage transmission network.

Report Outline

This subsection introduces the outline of the remaining chapters in this study. Chapter II focusses on the theoretical background and the system configuration of DFIG based wind power systems, most of the concepts presented there are generic and not tailored to suit any specific model of the systems under discussion.

Chapter III takes two main models of wind power systems, one average model available within the SimPowerSystems® blockset of MATLAB Simulink® and another detailed model that comes as a demonstration system within OPAL-RT's Artemis blockset. These are used to build a number of wind farms and integrated into a demonstration high voltage (HV) transmission system in Artemis.

The results of simulating the resulting system in real-time are shown and discussed in Chapter IV and finally, conclusions drawn from the study are discussed in Chapter V.

CHAPTER II

SYSTEM CONFIGURATION

Wind Turbine Characteristics

The horizontal axis wind turbine is the most common technology in practical use with units typically ranging from 500 kW to 5 MW. As illustrated in Fig. 2.1 a typical wind turbine has the following parts: Rotor (consists of blades and hub); drive-train (shafts, gearbox, couplings, mechanical brake, and electrical generator); nacelle and main-frame (housing, bedplate, and yaw system); tower and foundation; and electrical system (cables, switchgear, transformers, and power electronic converters if present) [12].

The major classifications of technologies in use for Wind Turbines are based mainly on their electromechanical components. The choice of technology has implications on cost, complexity and power extraction efficiency. The prime mover irrespective of the type generally consists of a blade and hub rotor assembly that is directly driven by the prevailing wind conditions and a drive-train assembly that is needed to step up the rotational speed needed to drive the generator. The generator serves as an electromechanical converter that transforms the mechanical energy into electrical energy. The real and reactive power output is then typically managed by power electronic converters. There are four basic types of wind turbines as follows [17] [18].

- Type 1: Fixed-speed wind turbines
- Type 2: Variable-slip wind turbines

- Type 3: Doubly-fed induction generator (DFIG) wind turbines
- Type 4: Full-converter wind turbines

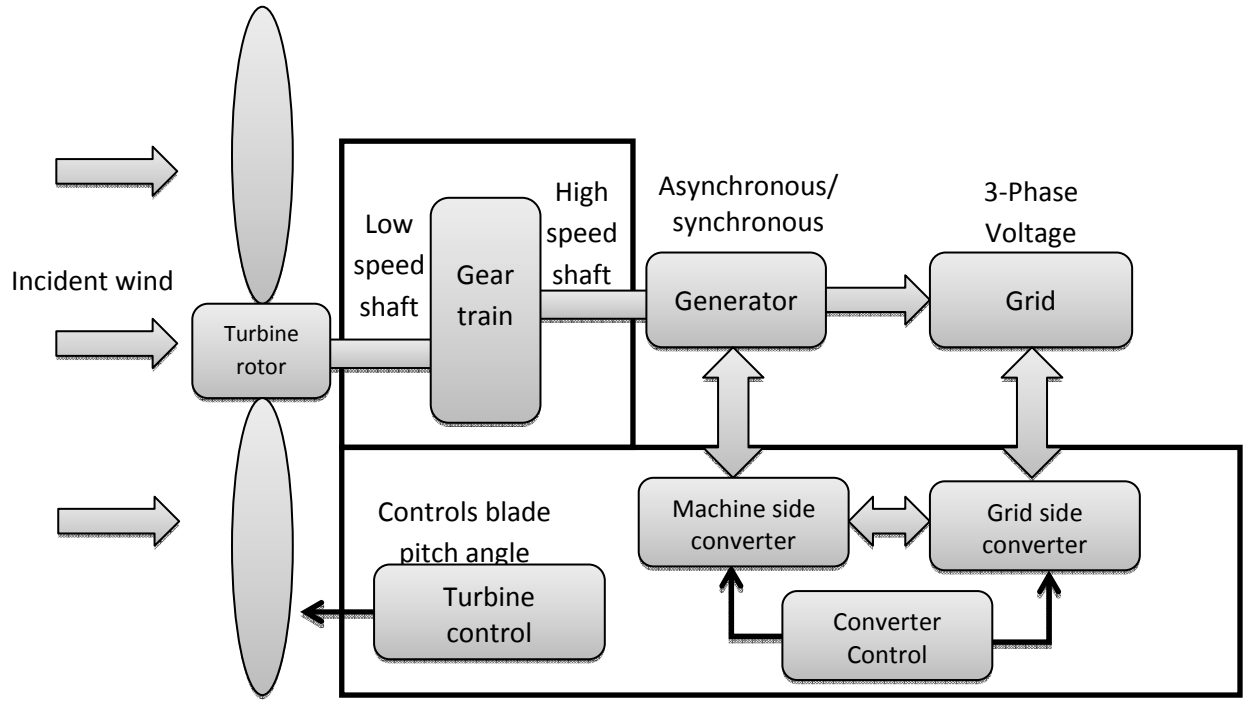

Fig. 2.1 Wind turbine diagram.

Fixed-speed wind turbines, as the name suggests, operate with minimal variation in turbine rotor speed since they employ a grid-connected squirrel-cage induction machine. Their simplicity of design makes them the basic utility-scale wind turbines in operation characterized by their robustness and reliability. They are however not the generator of choice due to their limited capabilities in energy capture; the requirement of additional mechanisms for reactive power compensation and suboptimal power extraction. Variable-speed wind turbines are able to overcome these shortfalls thus their dominance in practical applications. They are designed to operate over a wide but finite range of rotor speeds, and they usually employ blade-pitching as a means to maximize the cut-off speed of their operation. The cut-off speed is the maximum

operating wind speed of the wind turbine. Maximum power extraction greater than typically attainable with fixed speed wind turbines is attainable through speed and power controls. There is a wider range of operating slip speed (up to 10%) due to the employment of Variable-slip (VS) or dynamic rotor resistance (DRR) turbines that control the resistance in the rotor circuit of the machine. The main disadvantage of variable speed wind turbine is significant loss of efficiency due to energy lost as heat in the rotor resistance [12].

Doubly-fed induction generator (DFIG) turbines are variable speed wind turbines that are able to operate at minimal heat loss by employing a back-to-back AC/DC/AC converter in the rotor circuit to recover the slip power. Real and reactive power outputs are decoupled through flux-vector control of rotor currents. This also leads to maximized wind power extraction and lowering of mechanical stresses. The stator side is directly connected to the grid and thus the converter only handles the power in the rotor circuit. The converter rating is therefore below the full machine rating since it is limited to only the rotor side power [2] [12].

Wind Power System Modeling

The DFIG system is able to support a variable speed operation over a large but finite range whilst producing a constant frequency output. This is because of the ‘doubly fed’ configuration in which the voltage on the stator is applied from the grid and the voltage on the rotor is induced by the rotor-side converter. The frequency difference between the mechanical frequency (rotor side) and the electrical frequency (stator side) is compensated through a converter that injects a variable frequency rotor current both in normal and fault condition operation [19].

Aerodynamic Model for Rotor

The mechanical power extracted from a wind turbine, P_T, is dependent on the power coefficient, C_P, for the given turbine operation conditions and is given by [8] [12]

$$P_T = \frac{1}{2} C_P A \rho v^3 \tag{2.1}$$

where

C_P = Power coefficient (maximum value Betz's limit 0.593)

A = The area swept by the blades of the wind turbine

ρ = Specific air density

v = Wind speed

All other factors remaining constant, the power extracted by the wind turbine is directly proportional to C_P all other terms being constant. Excessively high wind speeds could cause the turbine to operate at higher than rated power output. This exposes the turbine to premature wear and tear on the turbine components thus shortening its operating life. One of two techniques may be employed to prevent this undesirable situation. If stall regulation is employed, a drag build-up limits the net mechanical power extracted during periods of excessive wind speeds. This is inefficient since the cut off wind power that could have been captured is lost to the system. Its simplicity and ability to function without the use of extra controllers makes it cost-effective. The alternative scheme is pitching. Here, the angle of the tip of the rotor blade or the entire blade is rotated in order to control the angle of attack, thus limiting the speed of rotation while extracting the maximum available power. Pitch controlled turbines are more efficient than stall controlled turbines; however they require additional controllers and components leading to relatively higher complexity and cost. Blade-pitching is the technique used here and thus, C_P is a function of the

pitch angle of turbine rotor blades, β, and the tip-speed ratio, λ, which is the ratio of the blade-tip linear speed to the wind speed is defined as [8] [12][12, 8]

$$\lambda = \frac{\omega_T R_T}{v} \tag{2.2}$$

where

ω_T = Rotor angular speed (rad/s)

R_T = Rotor radius of the turbine blade (m)

The power captured by the rotor of the wind turbine is therefore

$$P_T = \frac{1}{2}\rho \cdot C_P \cdot \pi R_T^2 \cdot v^3 \tag{2.3}$$

Also, the aerodynamic torque is given by:

$$T_r = \frac{\frac{1}{2}\rho \cdot C_P \cdot \pi R_T^2 \cdot v^3}{\omega_T} \tag{2.4}$$

Fig. 2.2 demonstrates the fact that for any given wind speed there is a corresponding generator speed that maximizes the power extracted by the generator. This helps to attain the generator power characteristic curve as illustrated in Fig. 2.3. The power characteristic therefore helps to follow the peak point on the power curve by regulating generator speed. The maximum power extracted is represented in equation 2.5.

$$P_{Tmax\_pu} = k_p v_{pu}^3 = k_p \omega_{T\_pu}^3 = k_{opt} \omega_{G\_pu}^3 \tag{2.5}$$

where $k_{opt} = k_p / 1.2^3$

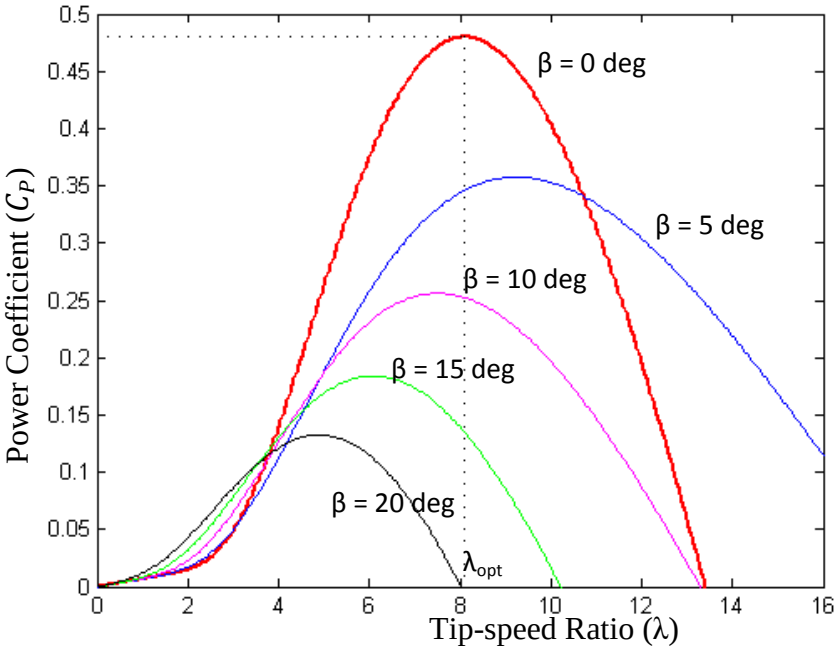

Fig.2.2 Power coefficient versus tip-speed ratio [8]

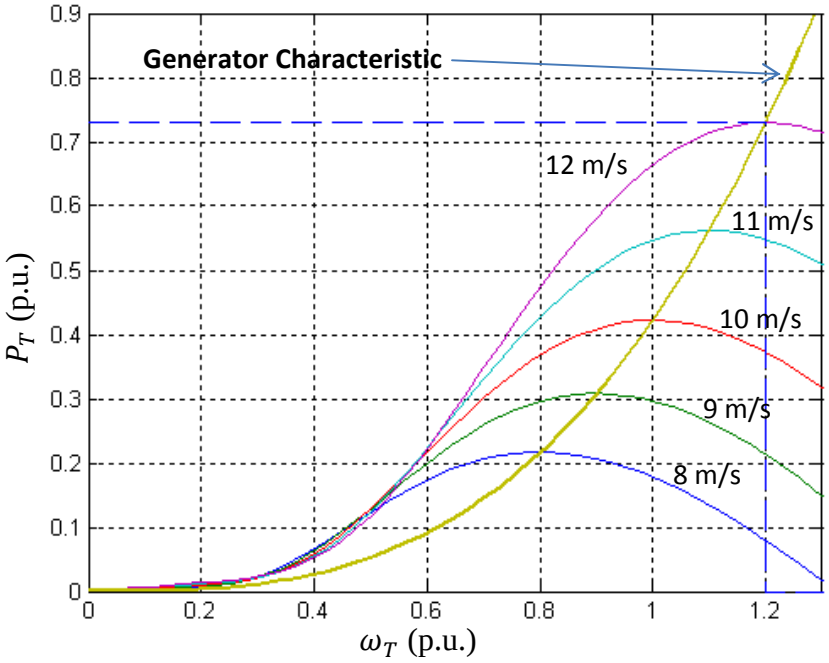

Fig. 2.3 Power characteristics of a wind turbine for various wind speed [8].

Torque Control

The torque is calculated based on the prevailing wind speed which is modeled according to a reference input speed by the user. In order to increase the rated power of the wind turbine, there is need to increase the blade length and by so doing increasing the area swept by the rotor blades. However in order to maintain low levels of audible noise the increasing rotor blade length also calls for operation at slower revolutions per minute. There turbine blade assembly is therefore connected to a mechanical drive train (typically a gear system) that internally steps up the shaft speed at which the induction generator operates [12].

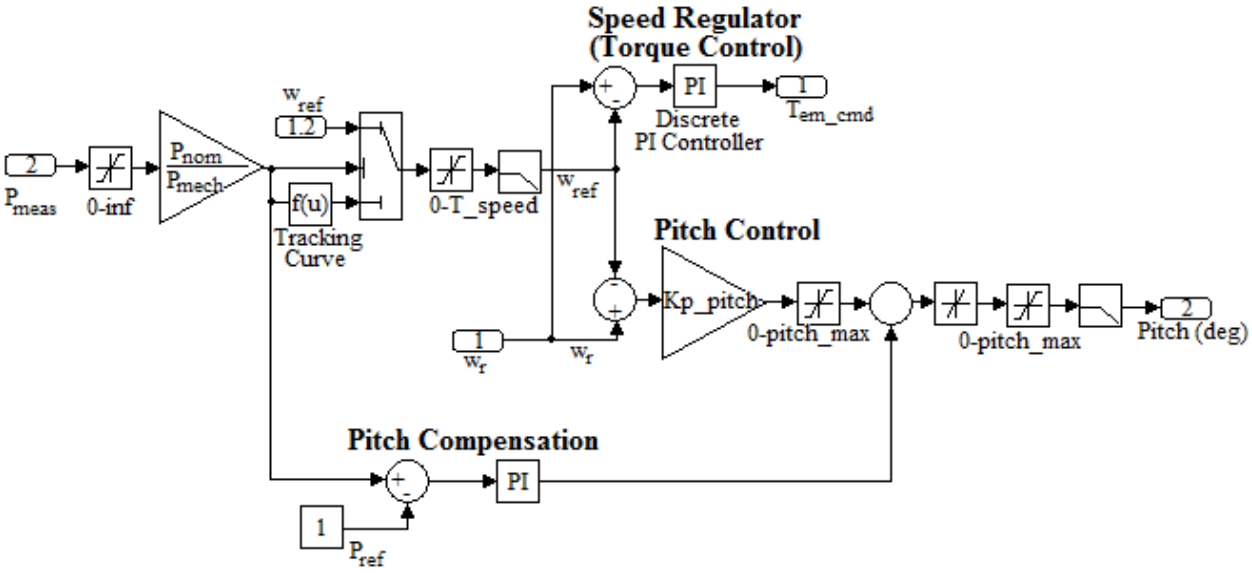

Fig. 2.4 Aerodynamic torque control

The pitch angle controller specifically comes into operation only in event that the input wind power exceeds the rated machine power, since under such conditions the rotor speed cannot be controlled by increasing the generator power without causing damage [19]. The pitch controller varies the angle of attack of wind onto the turbine blades and by so doing limits the

maximum power extracted to the rated wind generator maximum wherever the input mechanical power exceeds rated power. One possible implementation of this is to per-unitize the rated power and convert it into a reference speed. A PI controller compares the reference and actual in order to drive the input speed towards the reference. In addition an outer PI controller drives the input power towards the reference power through a pitch compensator system. Fig. 2.4 illustrates the combination of the speed regulator consisting of the pitch control and the pitch compensator [20].

Induction Generator Model

The generator effect is achieved when a rotating electrical machine produces electrical output power as a result of the mechanical power input from a prime mover. When induction machines are operated at speeds above their synchronous speed they act as generators, otherwise they act as motors [12]. In the DFIG, the stator is connected directly to the grid and it provides for variable speed operation through a partially rated rotor side converter [8]. As demonstrated in Fig. 2.5 the basic structure of the DFIG WG system, the back-to-back PWM converter consists of two converters that operate independently of each other. In this case, the rotor-side converter controls active and reactive power through rotor current regulation whilst the stator-side converter permits the operation at unity power factor (zero reactive power) through DC-link voltage regulation. In an over-synchronous condition the rotor feeds power via the converter to the grid whereas the rotor draws power during sub-synchronous operation. The stator on the other hand feeds power to the grid in either operational mode [21].

This principle is at the core of the DFIG based wind turbine and thus they are modeled as wound-rotor induction generators together with their associated input and output power

electronic circuits that regulate mechanical input power and electrical output power. These also help to achieve real and reactive power control, thus creating the possibility of using the wind turbine generator as a means of reactive power control. While the stator is directly connected to a three phase supply voltage (typically 1kV at 60Hz), the rotor is accessible through slip rings or brushes. The variably frequency power generated by the rotor is rectified and tied into the supply voltage through a back-to-back AC-DC-AC power electronic converter. This permits independent excitation of the rotor and stator circuits and permits the use of power electronic circuits rated only about 20% - 30% of the rated turbine output, since the power electronics circuit only carries the power generated through the rotor windings. By regulating the rotor winding current, the real and reactive power can be regulated by a separate control system in order to extract the maximum possible power from the input mechanical wind power. The common control methods for the DFIG based wind turbine mainly use vector/field-oriented control or direct torque control (DTC) with the former being more commonly used. It allows the real power control to be decoupled from reactive power control such that it is possible for the wind turbine to compensate for voltage drops without affecting their output real power [2, 8, 12].

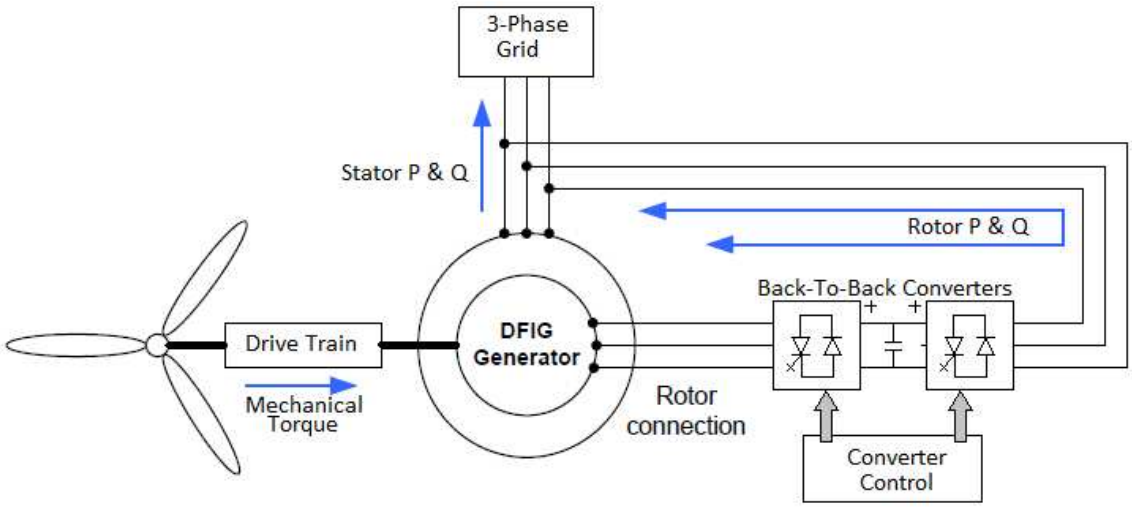

Fig. 2.5 Structure of DFIG wind power generation system.

In contrast with the squirrel-cage induction motor that has its rotor short-circuited hence making rotor power inaccessible, the rotor of the DFIG is accessible even though the power operates at a different frequency from the stator power. This is due to the fact that the output voltage from the rotor is as a result of the net flux linkage of the variable frequency variable magnitude PWM converter AC voltage input and the flux of the rotor rotating at the wind speed stepped up by the drive train. The resulting variable frequency rotor output power needs to be converted to the same frequency as the grid power through AC-DC-AC power converters, and thus an additional cost overhead [22]. The additional cost of the DFIG based wind turbine over a less controlled or uncontrolled generator such as a squirrel-cage induction based machine is compensated by several significant advantages such as independent active and reactive power control; a much larger range of generator shaft speed up to 30% above and below rate speed with minimum slip losses; pitch control permits maximum extraction of aerodynamic power and reduction of mechanical stress; and improved fault ride-through performance.

Compared to full-converter machines that need their AC-DC-AC converters rated at 100% of the rated turbine output power, the lower rating (20% to 30% of rate turbine output power) makes is a more cost-effective alternative. In addition, since DFIG is an induction machine, its electrical dynamic performance at fundamental frequency is dominated by the power converter rendering conventional aspects of generator performance such as internal angle, excitation voltage, and synchronism irrelevant [12].

The DFIG system is able to support a variable speed operation over a large but finite range whilst producing a constant frequency output. This is because of the ‘doubly fed’ configuration in which the voltage on the stator is applied from the grid and the voltage on the

rotor is induced by the rotor-side converter. The frequency difference between the mechanical frequency (rotor side) and the electrical frequency (stator side) is compensated through a converter that injects a variable frequency rotor current both in normal and fault condition operation [19]. A DFIG consists of a WRIG with the stator and rotor windings. The stator and rotor voltage equations of a wounded rotor induction generator in the d-q reference frame are as follows [23] [24]:

$$v_{ds} = R_s i_{ds} - \omega_e \varphi_{qs} + \rho\rho\varphi_{ds} \tag{2.6}$$

$$v_{qs} = R_s i_{qs} - \omega_e \varphi_{ds} + \rho\varphi_{qs} \tag{2.7}$$

$$v_{dr} = R_r i_{dr} - (\omega_e - \omega_r)\varphi_{qr} + \rho\varphi_{dr} \tag{2.8}$$

$$v_{qr} = R_r i_{qr} + (\omega_e - \omega_r)\varphi_{dr} + \rho\varphi_{qr} \tag{2.9}$$

The instantaneous power input of the rotor and stator in the d-q reference frame is [2] [3]

$$P_s = -\frac{3}{2}\omega_e\left(\varphi_{qs} i_{ds} - \varphi_{ds} i_{qs}\right) \tag{2.10}$$

$$P_r = -\frac{3}{2}(\omega_e - \omega_r)\left(\varphi_{qr} i_{dr} - \varphi_{dr} i_{qr}\right) \tag{2.11}$$

Fig. 2.6 illustrates the independent real and reactive power control achievable in the DFIG-Based wind power system. It can be observed that a real power jump or drop has no effect on the steady state reactive power. Likewise a reactive power jump or drop does not affect the real power output. This effect is made possible through the grid-side and rotor-side converter controls. The grid-side and rotor-side converters are discussed subsequently.

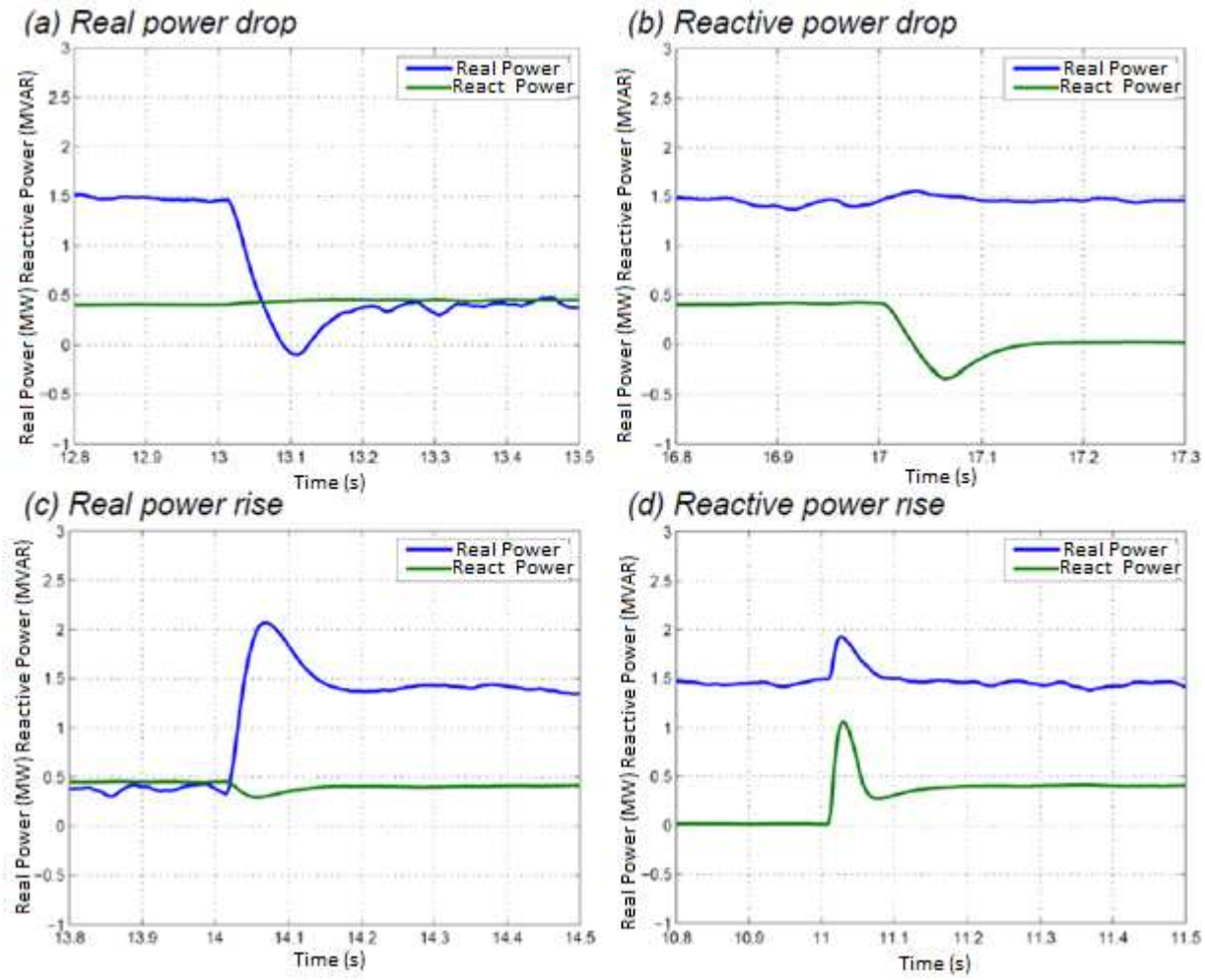

Fig. 2.6 Independent real and reactive power control [12]

Grid-Side Converter

The role of the grid-side converter is to maintain a constant DC-link voltage under conditions of changing rotor power magnitude and direction. It uses a current regulated PWM scheme in which the d-q reference frame currents are used to regulate DC-link voltage and reactive power [25]. The schematic structure of the stator-side converter is as show in Fig. 2.7. It is an implementation of the stator-flux oriented vector control scheme and thus permits separate

real and reactive power control. Based on the connection of the inductance and resistance in Fig. 2.7, the inductor voltage can be written as shown in equation 2.12 [26].

$$\begin{bmatrix} v_{as} \\ v_{bs} \\ v_{cs} \end{bmatrix} = R \begin{bmatrix} i_{as} \\ i_{bs} \\ i_{cs} \end{bmatrix} + L\rho \begin{bmatrix} v_{a1} \\ v_{b1} \\ v_{c1} \end{bmatrix} \tag{2.12}$$

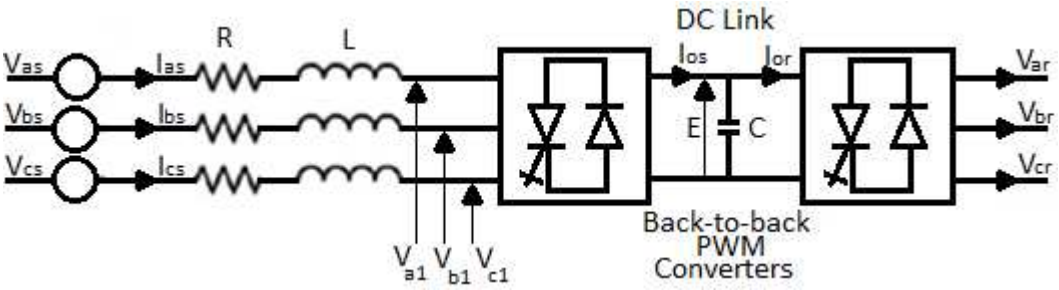

Fig. 2.7 Back-to-back converter connection

Equations 2.13 and 2.14 show how the reference values of the stator side converter are calculated. It is evident that the d-q axis reference frame components are independent and can thus be controlled separately [12].

$$v_{d1}^{*} = -v_d + \left(\omega_s L i_q + v_d\right) = -v_d + v_{d1}^{comp} \tag{2.13}$$

$$v_{q1}^{*} = -v_q + \left(\omega_s L i_d\right) = -v_q + v_{q1}^{comp} \tag{2.14}$$

A typical stator-side converter controller is illustrated in Fig. 2.8. It uses the close-loop control scheme to maintain a constant DC-Link voltage by calculating the stator flux from the terminal quantities [12].

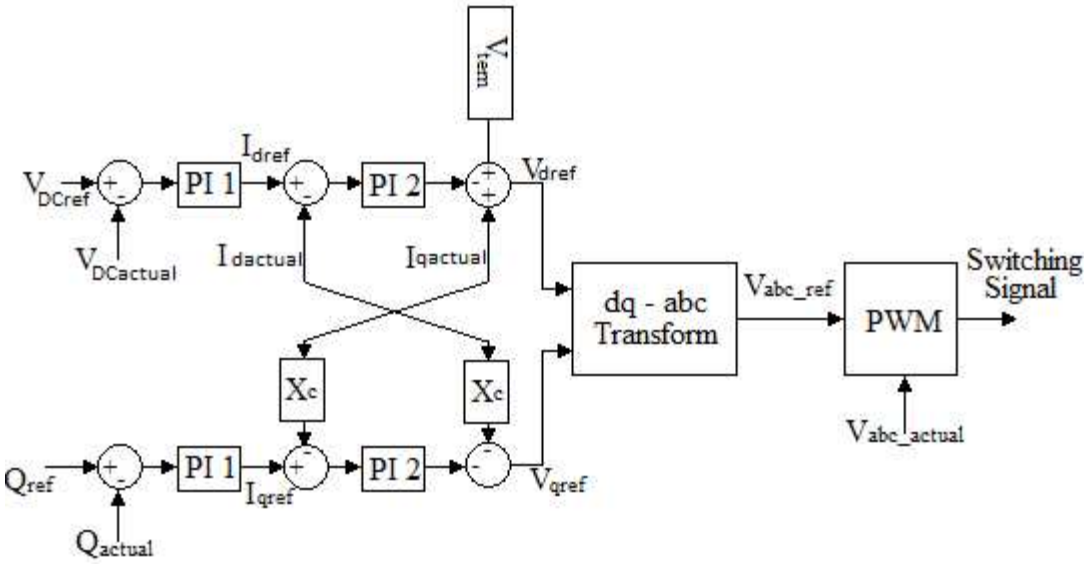

Fig. 2.8 Stator-side converter control

Rotor-Side Converter

The rotor side converter control independently controls the electromagnetic torque and the rotor excitation current. The control scheme is presented along the stator-flux linkage making the q-axis flux component on the d-q reference frame zero. In addition, the stator resistance is negligible since it is grid-connected and thus the d-axis flux component is assumed constant. The rotor voltages are redefined for decoupled control summarized as follows [12].

$$v_{dr} = v'_{dr} + v_{dr}^{comp} \tag{2.15}$$

$$v_{qr} = v'_{qr} + v_{qr}^{comp} \tag{2.16}$$

$$v'_{dr} = R_r i_{dr} + \sigma(L_{lr} + L_m)\rho i_{dr} \tag{2.17}$$

$$v'_{qr} = R_r i_{qr} + \sigma(L_{lr} + L_m)\rho i_{qr} \tag{2.18}$$

$$v_{dr}^{comp} = \frac{L_m}{L_{ls}+L_m}\rho\varphi_{ds} - (\omega_e - \omega_r)\sigma(L_{lr} + L_m)i_{qr} \tag{2.19}$$

$$v_{qr}^{comp} = (\omega_e - \omega_r)\frac{L_m}{L_{ls}+L_m}\varphi_{ds} - (\omega_e - \omega_r)\sigma(L_{lr} + L_m)i_{dr} \quad (2.20)$$

Since the rotor side compensation terms are independent of each other thus permitting independent control of each axis reference frame using its corresponding current. The rotor converter control is based on the stator flux orientation hence stator-flux oriented vector control of the rotor side. A typical rotor-side converter control based on equations 2.15 to 2.20 is demonstrated in Fig. 2.9.

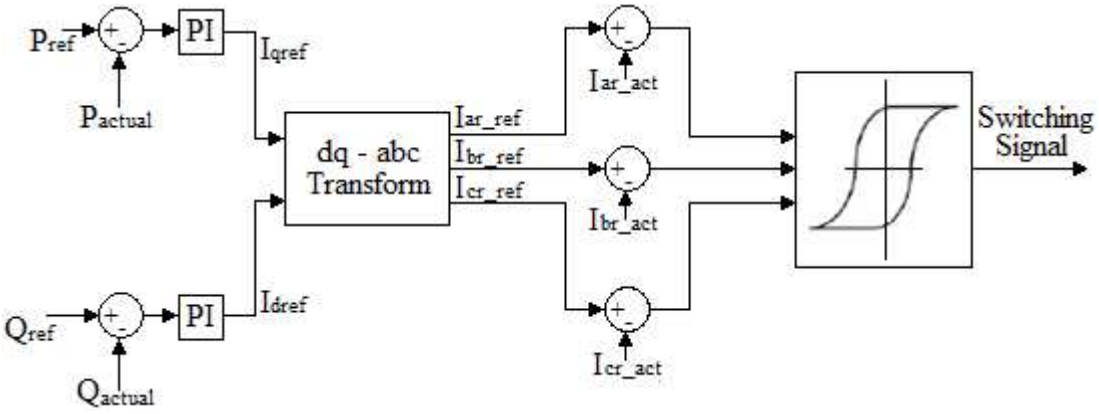

Fig. 2.9 Rotor-side converter control

CHAPTER III

SIMULATION SETUP

Simulation Environment

A real-time simulation is performed in predefined time steps and the rate of generation of outputs at each time step is not based on the speed of computation but rather on the real-time pace of data generation if it were replaced by the actual physical system being modeled. Within the fixed time step the simulator has to read in all inputs such at sensor readings, perform all necessary computations including control algorithms, and to write out all necessary analog/digital outputs. In the situation where the time step is insufficient for all these processes it leads to overruns. A higher time step could be used to overcome this but increasing the time step also decreases the accuracy of the system's approximation to the real physical system; a trade-off thus needs to be made.

eMEGASim® PowerGrid Real-Time Hardware in the Loop Simulator is an integration of OPAL-RT's powerful electrical circuit solvers, SimPowerSystem blockset of MATLAB and RT-LAB distributed processing software and hardware platform. These ensure a high speed real-time simulation environment for both small and large power systems. There are customizable inputs and outputs on the hardware platform that permit the integration of real power system hardware in the software loop of the simulator and these are driven by specialized solvers specifically designed for the eMEGASim® platform. The setup used in this study consisted of the OP5600 hardware platform and RT-LAB distributed processing software that used ARTEMiS solvers for

real-time model computation. The details of the hardware and software components are discussed in the following subsections.

Hardware Details

The author used OP5600 digital simulator to demonstrate the real-time performance of both average and detailed model of wind power generators [27]. It is built using low cost, high availability commercial-off-the-shelf (COTS) components that includes advanced monitoring capabilities and scalable input/output (I/O) and processor power. This is because of its modular flexible design that permits full customization aimed at a wide range of specific I/O requirements [28].

The eMEGASim® simulator contains a powerful real-time target computer equipped 12 3.3-GHz processor cores running Red Hat Linux real-time operating and two user-programmable FPGA-based I/O management options available, powered by the Xilinx Spartan-3 or more powerful Virtex-6 FPGA processor. Available expansion slots accommodate up to 8 signal conditioning and analog /digital converters modules with 16 or 32 channels each for a total of fast 128 analog or 256 discrete or a mix of analog and digital signals [28].

There are four available targets that can be networked into a multiple-target PC cluster or for complex applications capable of implementing large models with more than 3000 I/O channels and a time step below 25 micros. This also allows including hardware-in-loop (HIL) testing, complex power grids, micro-grids, wind farms, etc. can be simulated with time step as low as 10 microseconds or less than 250 nanoseconds for some subsystems in order to maximize accuracy. It also offers versatile monitoring on the front panel through RJ45 to mini-BNC connectors [28].

Fig. 3.1 shows the front and back views of the OP5600 digital simulator. Each target OP5600 Chassis has an upper section of I/O signal modules including converters/conditioners and a bottom section that contains the multi-core processor computer. This runs the target's operating system that includes an installation of OPAL-RT's real-time simulator system including RT-LAB. Monitoring interfaces and monitoring connectors are accessed through the front of the OP5600 Chassis, while access to all I/O connectors, power cables and the main power switch are accessible on the back of the OP5600. The OP5600's design also includes an option to connect up to 16 single-ended signals on Mini-BNC connectors, making it easy to monitor signals using an oscilloscope while the systems is in used and connected to user equipment [28].

Front View Back View

Fig. 3.1 OP5600 Real-Time Simulation Target

Software Details

The power system components used to simulate the power system come from MATLAB Simulink's SimPowerSystem® Toolbox. The Real-Time Solvers for electromechanical system simulation come from the ARTEMiS Toolbox that are also targeted to the OP5600 digital

simulator. The enhanced algorithms used in ARTEMiS ensure reliable, accurate and fast fixed-step length computations essential for high fidelity, high-performance simulations. These are the requirements for which the ARTEMiS solver was designed and build in order to support real-time implementations of power systems simulations leading to significant improvement in speed without compromising accuracy.

The ARTEMiS solvers are proven to be highly accurate and stable over much larger time steps than with the Trapezoidal fixed-time-step algorithms used by Simulink. Users can therefore get the same accuracy with less powerful and lower-cost systems, to give the performance needed for high-fidelity real-time simulation. Furthermore, ARTEMiS includes special power-circuit-specific algorithms for addressing typical problems encountered when converting your SimPowerSystems model to real-time. For example, for circuits with switches, ARTEMiS calculates all circuit topology matrices prior to running the simulation, and uses circuit decoupling methods to reduce the size and number of these matrices, so that the computation runs smoothly in real-time, even when a switch changes state. Similarly, strategies to avoid algebraic loops and non-deterministic iterative calculations are included. These allow fixed computation times per step and interruption-free simulation in real-time [29].

Fig. 3.2 is a one-line diagram of the power system used in this study. It was adopted from a demonstration model used in [29]. It consists of a 500 kV ac transmission network with 23 buses, 45 distribution lines, 7 hydraulic generation turbine plants (synchronous machines and regulators), and 17 loads. The nominal operating frequency of the network is 60 Hz. A wind farm consisting of a total of 65 wind turbines (doubly fed induction generators) is connected in the middle of the transport network. The details of the system are further discussed in subsequent subsections.

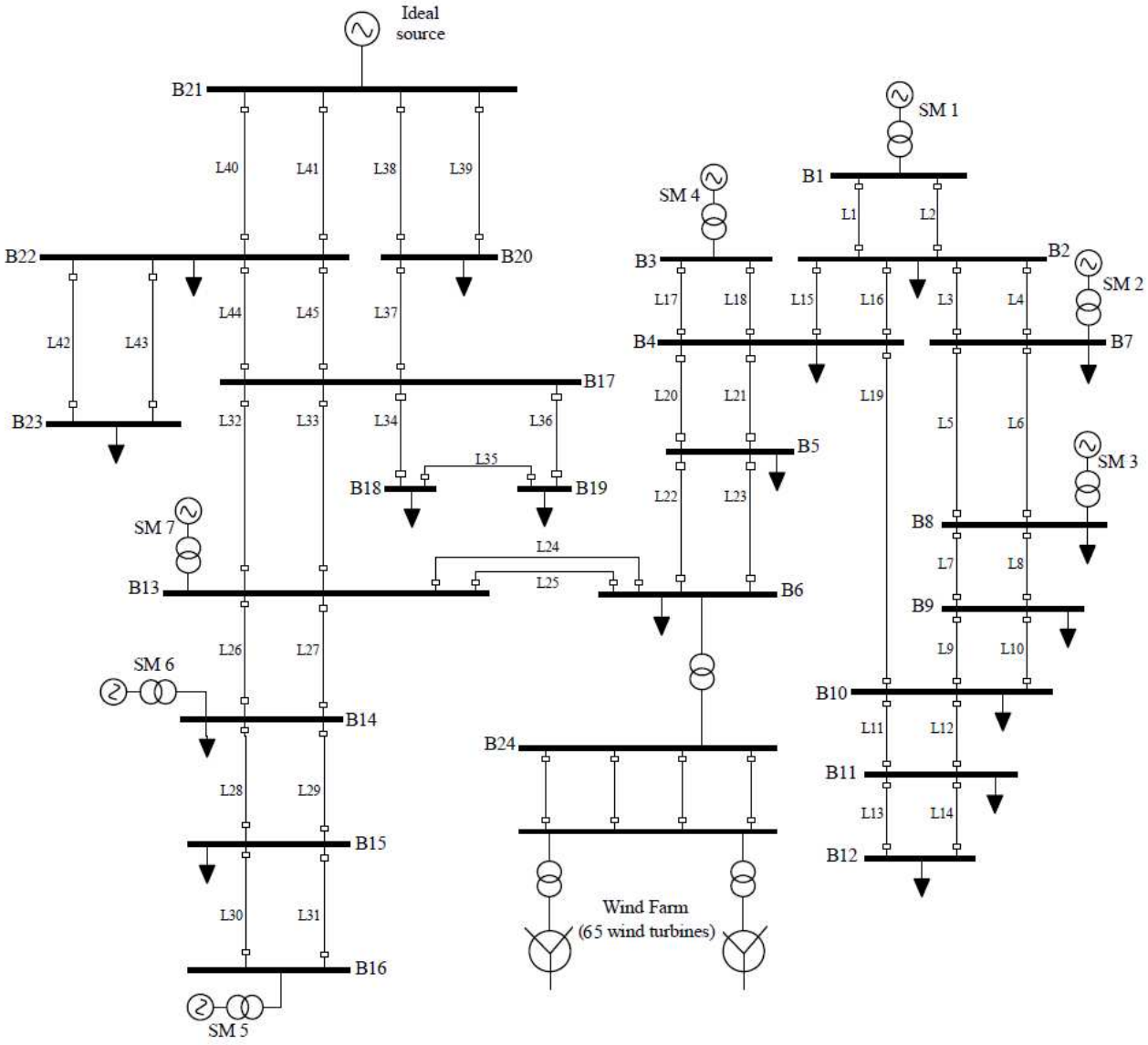

Fig. 3.2 One-Line diagram of the Wind Power Integrated Grid used in this study

Model Description

Transport Network

The transport network is divided into three subsystems namely “SM_NETWORK_A”, “SM_NETWORK_B” and “SM_NETWORK_C”. SM_NETWORK_A consists of the swing bus, buses13 to 23, seven (7) loads and three (3) hydraulic plants. Buses one (1) to six (6) are located in SM_NETWORK_B. This subsystem also consists of four (4) loads and a tie in to the wind farm. SM_NETWORK_C consists of buses seven (7) to twelve all load buses and two hydraulic plants.

Wind Farm

The wind farm is broken into four subsystems and connected as show in Fig. 3.3 to the transport network. The four subsystems have been designated as SS_WTGS1-4. Different options are available for modeling the individual wind turbine within these wind farms depending on the range of frequencies to be represented. Three simulation methods used to model Voltage-Sourced Converters (VSC) based wind power systems are average model, detailed model and phasor model.

In the average model, equivalent voltage sources are used to represent the IGBT VSCs. The AC voltage generated by these equivalent sources is averaged over one cycle of switching frequency. Harmonics are ignored but the dynamics associated with the control system and power system interaction are sustained. The average model is used to represent wind turbines in SS_WTGS_1 and SS_WTGS_3.

The detailed model is well suited for observing harmonics and transient behavior of the control system due to the inclusion of detailed representation of the power electronic IGBT

converters and its ability to operate at a high switching frequency range between 1620 Hz and 2700 Hz. The detailed model is used to represent wind turbines in SS_WTGS_2 and SS_WTGS_4. The phasor model is however not used in the network under study. It is the preferred modeling method where interest focusses on the low frequency mechanical oscillations over long periods of time (tens of seconds to minutes). It derives its name from the fact that it represents sinusoidal voltages and currents as phasor quantities.

Model Implementation

Description

Fig. 3.3 shows the Simulink implementation of the power grid used in this study. It was broken down into eight (8) subsystems according to the recommended OPAL-RT naming convention. A prefix of “SM_” indicates a master subsystem that serves as the program entry point for the simulation. “SS_” indicates a slave subsystem that is a subroutine accessed by the master subsystem. Both master and slave subsystems are compiled to run on the real-time simulation target. In contrast the “SC_” subsystem, which is the console through which the user is able to input variables into the system and also observe outputs, runs on the user workstation and communicates with the real-time target through a TCP/IP connection. Each master/slave subsystem is assigned to a specific CPU on the target as indicated in Fig. 3.3.

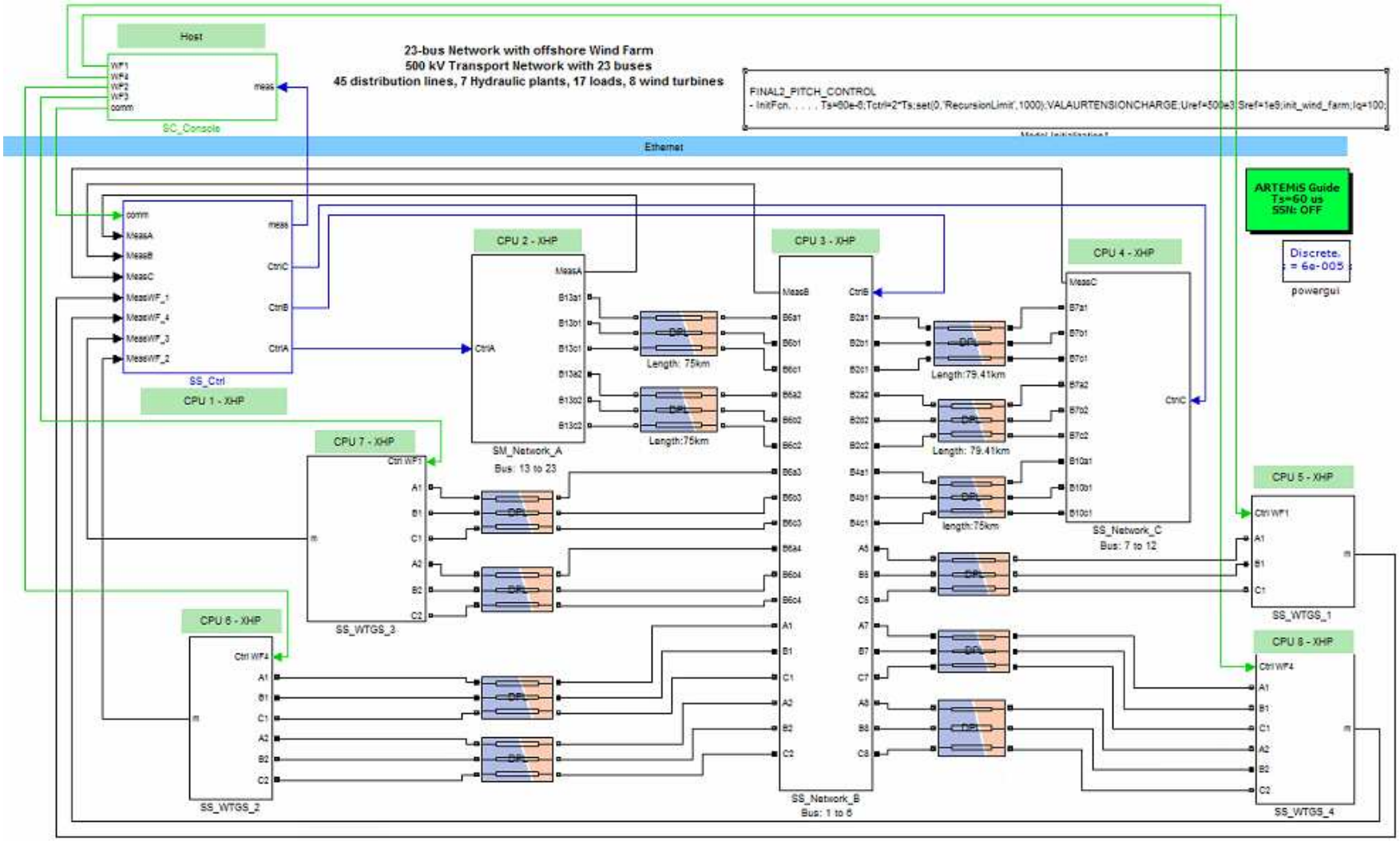

Fig. 3.3 Simulink Implementation of Wind Power Integrated Grid

Limitations

Simulating very large power systems in OP5600 digital simulator is limited by the number of processors available on the simulation target. In the case of this research, the maximum number of active processors licensed was eight (8) hence the power system could be broken into a maximum eight (8) subsystems. On the other hand, overloading any one subsystem also led to overruns since the computation time increased considerably.

It was observed that the stability of the model network was easily perturbed by minor configuration changes that led to overruns. For example, connecting a WTGS subsystem to any subsystem other SM_NETWORK_B led to excessive overruns affecting every other computational time step. In addition, the length of the longest path of transmission line within any given subsystem was limited since having excessively long transmission lines with excessively long time steps also led to overruns. The final network configuration used in this document was therefore chosen with these constraints in mind.

CHAPTER IV

RESULTS AND DISCUSSION

The power network model being simulated in this experiment was built and run in XHP mode on the OP5600 digital simulator. The build run at 80% of time step usage and no overruns. The next sections discuss the development and testing of the final model used in this study.

Model Development

The network illustrated in Fig. 3.2 with the wind farms was grouped into seven subsystems as indicated in Fig. 4.1. SS_WTGS_1 was connected to Bus 16 in SS_NETWORK_A, SS_WTGS_2 and SS_WTGS_3 were connected to Bus 6 to SS_NETWORK_B, whilst SS_WTGS_4 was connected to Bus 11 of SS_NETWORK_C. Several challenges arose with this initial configuration of the wind farms that let to excessive overruns in real-time simulation even though the model run offline successfully. These issues have been summarized below.

- SS_WTGS_1 and SS_WTGS_3 generated overruns due to an excessively long computation time brought about by their large number of wind turbines.
- SS_WTGS_2 and SS_WTGS_4 also generated overruns even though they had fewer models due to the higher complexity of the detailed models used in these subsystems.

- In addition, the remote location of SS_WTGS_1 and SS_WTGS_4 in the transport network increased the waiting times for their inputs and outputs.

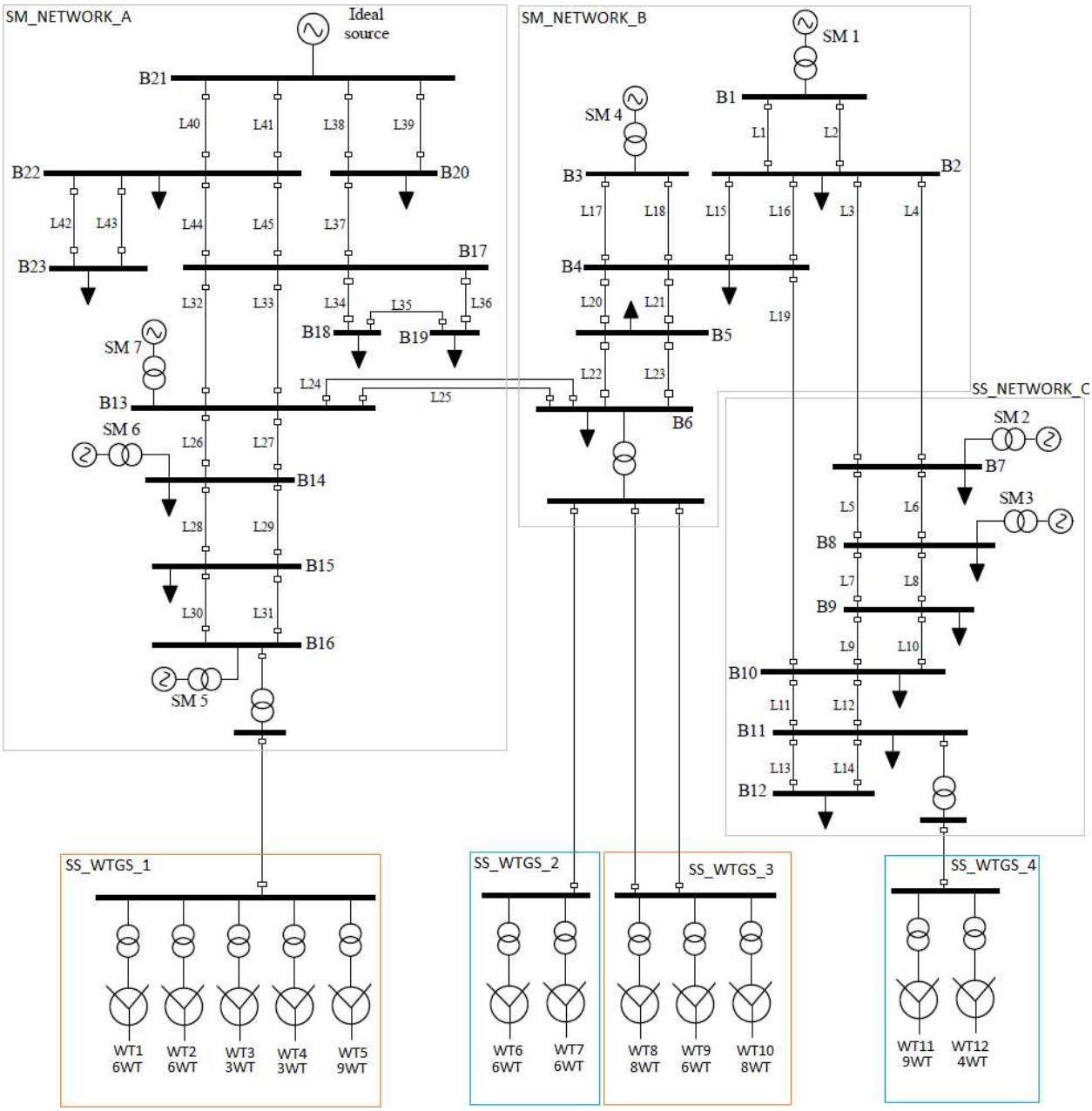

Fig. 4.1 Initial model configuration

In order to minimize the computation time of SS_WTGS_1 and SS_WTGS_3, the wind farms were consolidated into single average wind models that are current and voltage source approximations of the aggregate effect of the entire wind farms. Reducing the number of wind turbines in each of SS_WTGS_2 and SS_WTGS_4 meant a final 16 wind turbines for each wind farm. Finally the SS_WTGS_1 and SS_WTGS_4 were both moved to Bus 6 of SM_Network_B in order to minimize the waiting time between the subsystems. Fig. 4.2 represents the final model used in this study after making the above changes (Simulink model can be seen in Fig. 3.3.). This model compiled and ran with less than 80% of time step utilization and zero overruns.

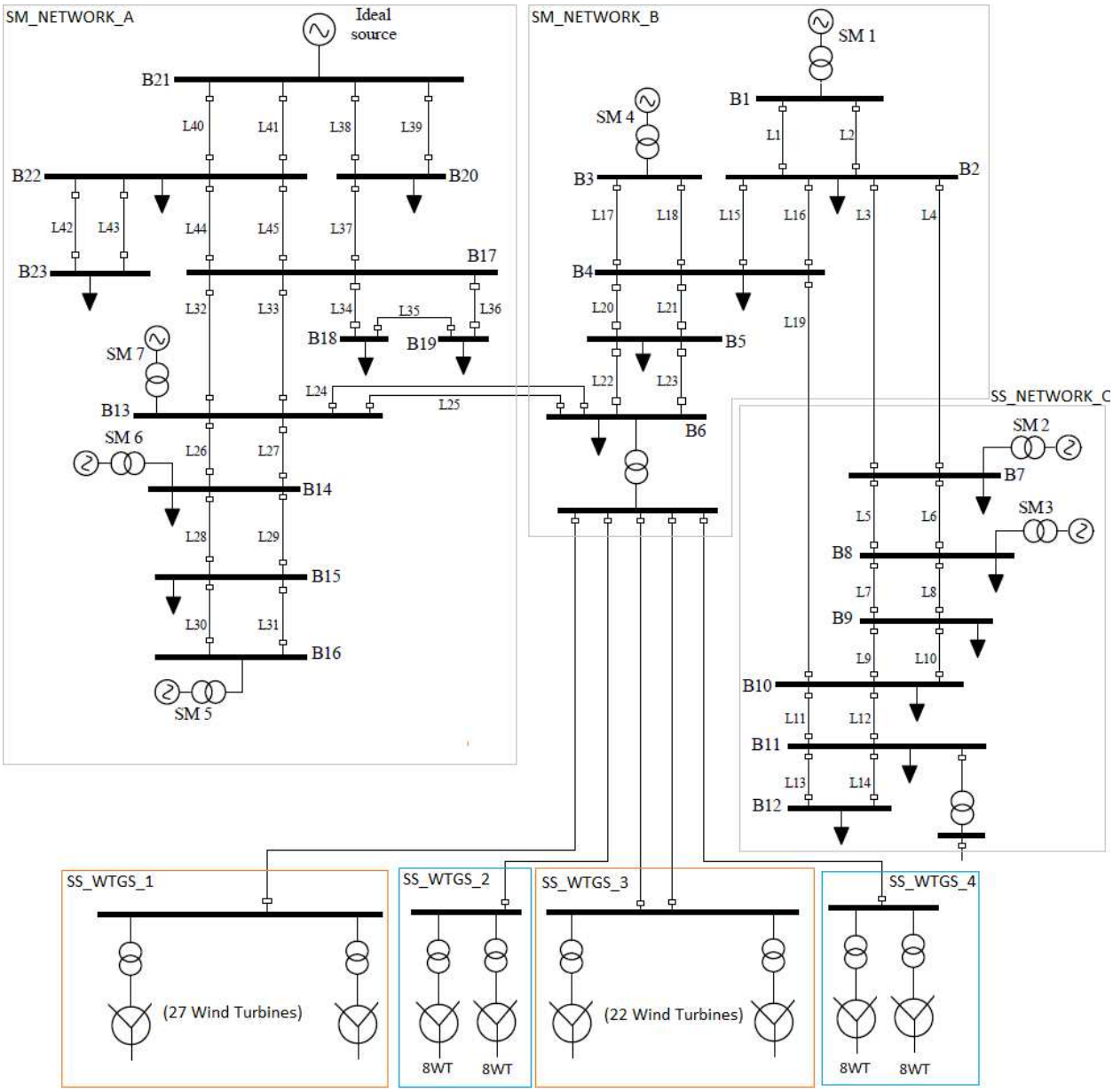

Fig. 4.2 Final model configuration

Model Testing

Both the detailed and average wind power models were tested in subsystems SS_WTGS_1-4 while grid-connected in so as to validate the model capabilities based on the following three major objectives adapted from [12].

- Verification of wind turbine power curve
- Independent real and reactive power control

The ability to satisfy these tests is seen as the basis to model more advanced controls such as inertia and frequency response [12]. In this study, the tests were performed with a simple average wind turbine model [30] shown in Fig. 4.3 and compared with the wind farms in the final model configuration of Fig. 4.2.

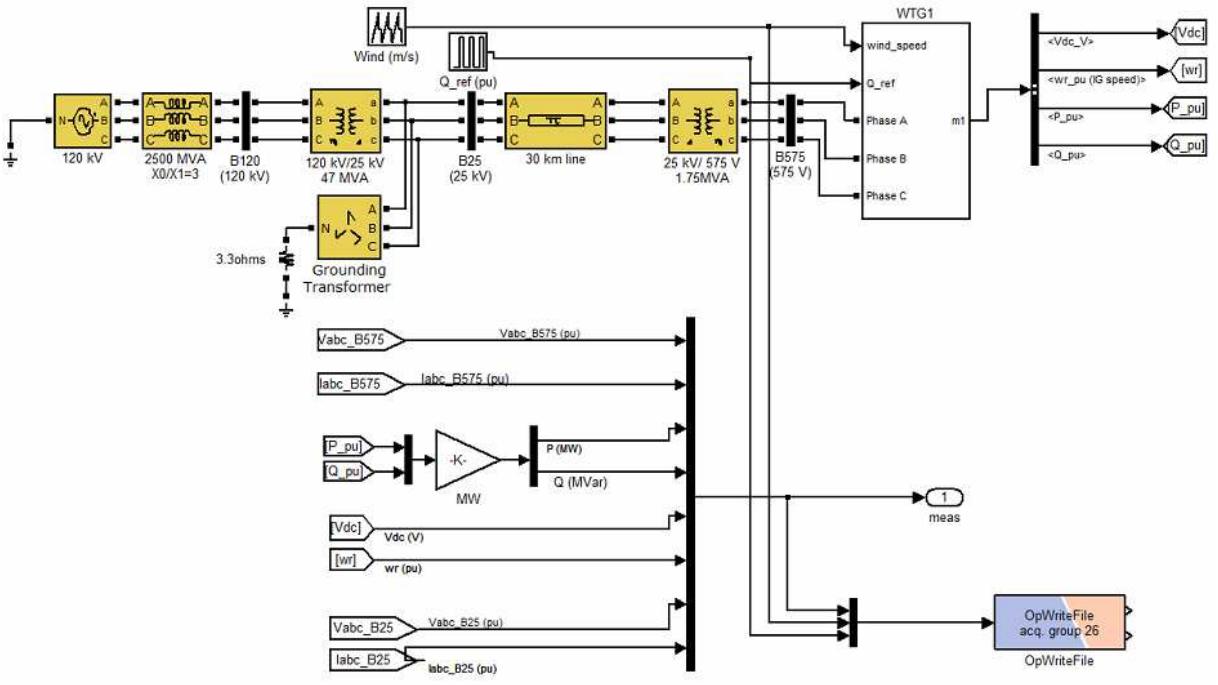

Fig. 4.3 Basic test system used in the study

Power Curve

The power curve for the model in Fig. 4.3 was attained by increasing the input wind speed from 0 m/s at time t=0 s to 20 m/s at time t=20 s. The resulting variation in real power is illustrated in Fig. 4.4. This is a close approximation of the theoretical power curve shown in Fig. 2.3.

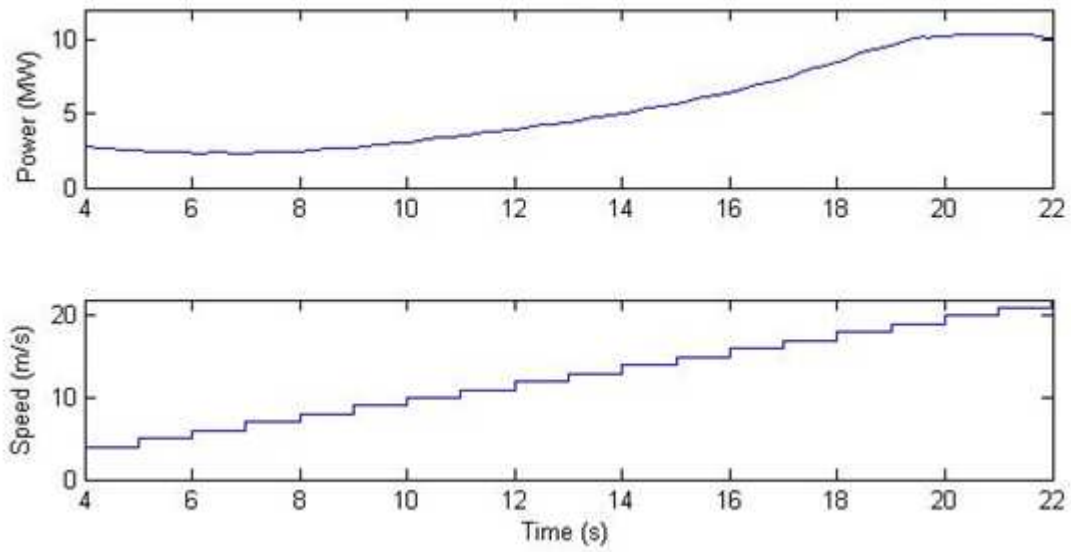

Fig. 4.4 Power curve for the basic test system used in the study

For the wind farms, input wind speed was varied linearly over time from 0 m/s at time t=4 s to 20m/s at time t=20 s for turbines in WTGS 2 and WTGS 3. Fig. 4.3 and Fig. 4.4 illustrate the change in output power over time for the average model of all wind turbines in WTGS 3 and a single detailed wind turbine in WTGS 2. The average model showed the desired power curve in contrast with the detailed model in which the relationship between the output power and input wind speed is not clearly defined.

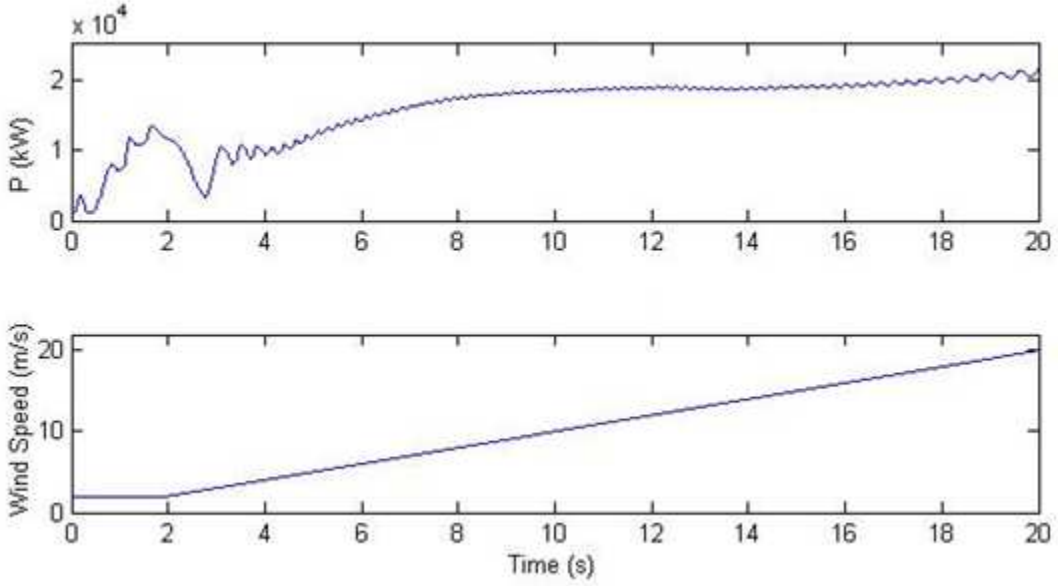

Fig. 4.5 Characteristic for WTGS 3

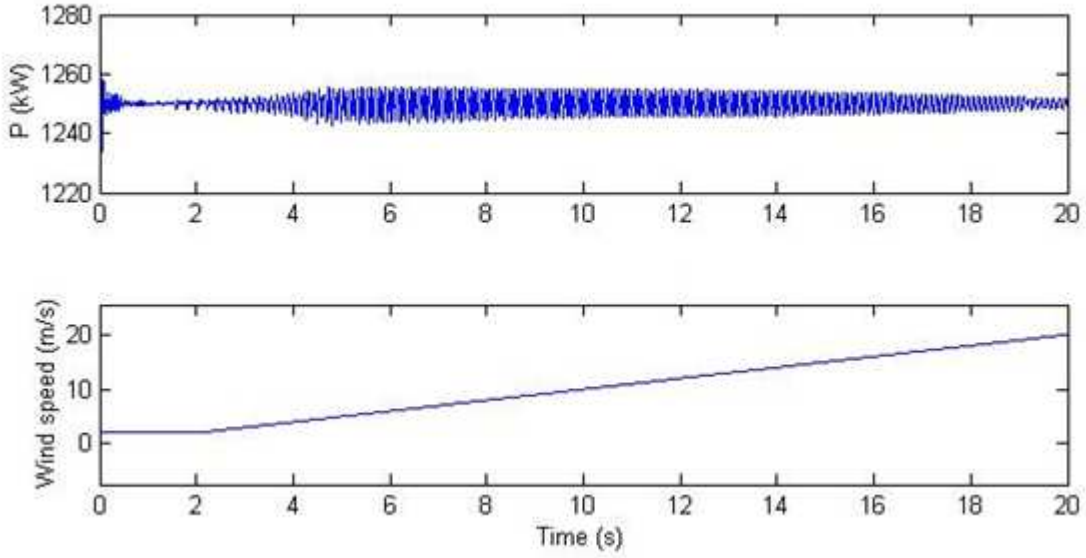

Fig. 4.6 Characteristic for WTGS 2

The real power output of the detailed WTGS model in Fig. 4.4 oscillates about the rated output power. The real power output of the average WTGS model in Fig. 4.3 oscillates before the cut-in speed of 4 m/s and then increases with increasing wind speed before flattening off at about 10 m/s; a typical power curve. Although both of these models have been tested independently to appropriately generate the desired output power curve, the detailed model failed in the case where it has been connected to the very large power system used in the case of this experiment. There are however no apparent computational reasons for this result since the model was simulated at below 80% time step utilization for all subsystems with zero overruns. The only conclusion that can be obviously derived is that the more complex detailed wind turbine model loses its stability when integrated into a large power system.

Independent Real and Reactive Power Control

To test the independent control of real power, the input wind speed was varied from 2 m/s to 20 m/s at times t=4 s and t=20 s while holding the reactive power reference at 0 p.u. The resulting output real and reactive power are illustrated in Fig. 4.7.

From Fig. 4.7 the varying wind speed caused a change in the real power output without affecting the reactive power output. The input wind speed was then held constant at 10 m/s while the reactive power reference was changed from 0 p.u. to 0.5 p.u. The resulting output real and reactive power are illustrated in Fig. 4.8. It can be observed that the real power output remained unchanged while the reactive power output increased in response to the increase in the reference power change.

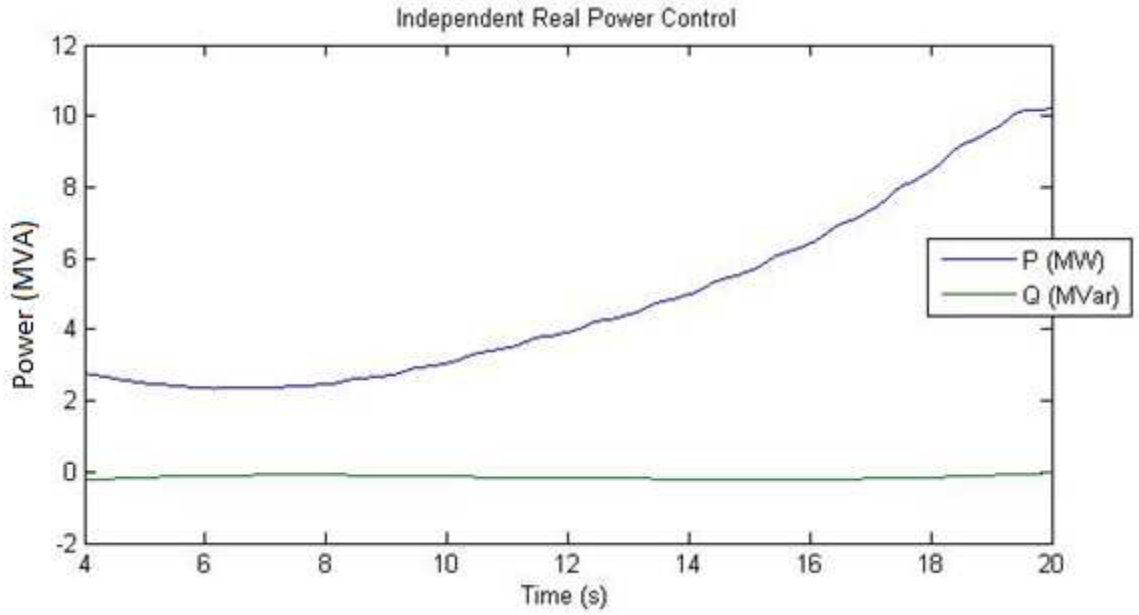

Fig. 4.7 Independent real power control for the basic test system

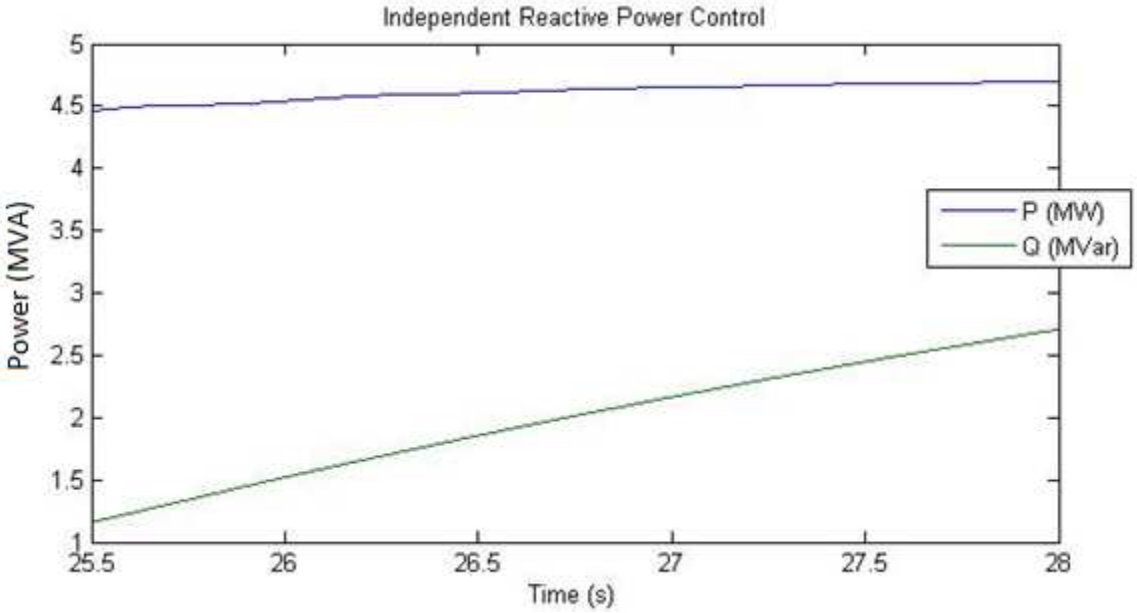

Fig. 4.8 Independent reactive power control for the basic test system

In testing for independent real power control for the wind farm, the wind speed was varied linearly from 2 m/s at time 2 s to 20 m/s at time 20 s for SS_WTGS_3 (for the average

model) and SS_WTGS_2 (for the detailed model) while holding reactive power reference at 0 p.u. The test for independent reactive power control involved holding a constant wind speed to 10 m/s for both SS_WTGS_1 (for average model) and SS_WTGS_4 (for detailed model) from 0 p.u. to 0.5 p.u at time t=20 s. In both the real and reactive power tests, the reactive power output remained unstable with either variation, an indication of possible controller instability while the wind turbine models are integrated into the power system. Fig. 4.9 illustrates the changes in output real and reactive power for WTGS 1 while holding wind speed constant and changing reactive power reference from 0 p.u. to 0.5 p.u. The output real power however is not constant and the reactive power is unstable, oscillating between -1 p.u. and 1 p.u. These challenges prevent the independent control of reactive power.

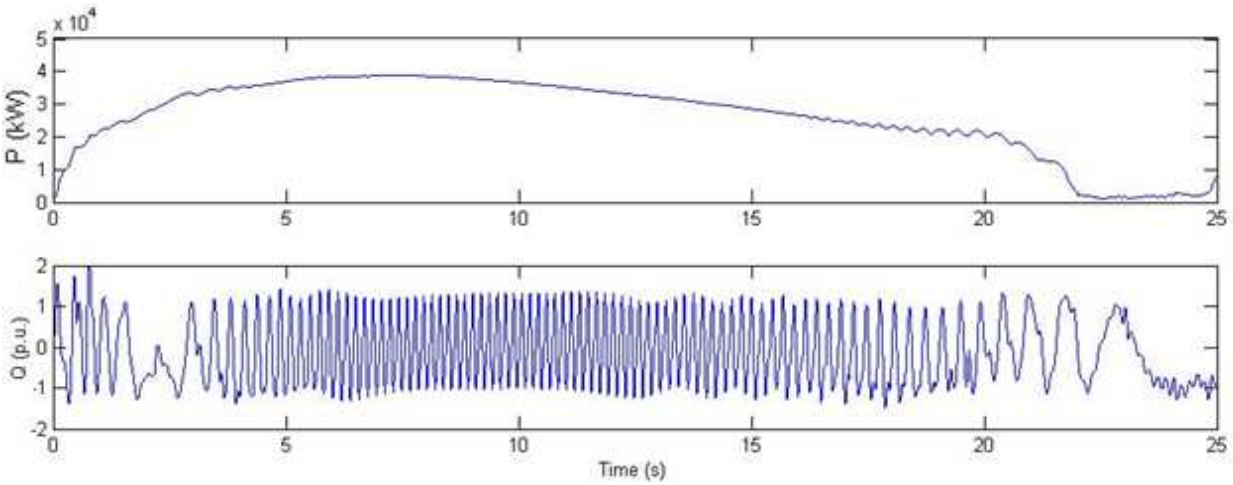

Fig. 4.9 Reactive Power Control for WTGS 1 (Challenges Pending with Independent Control)

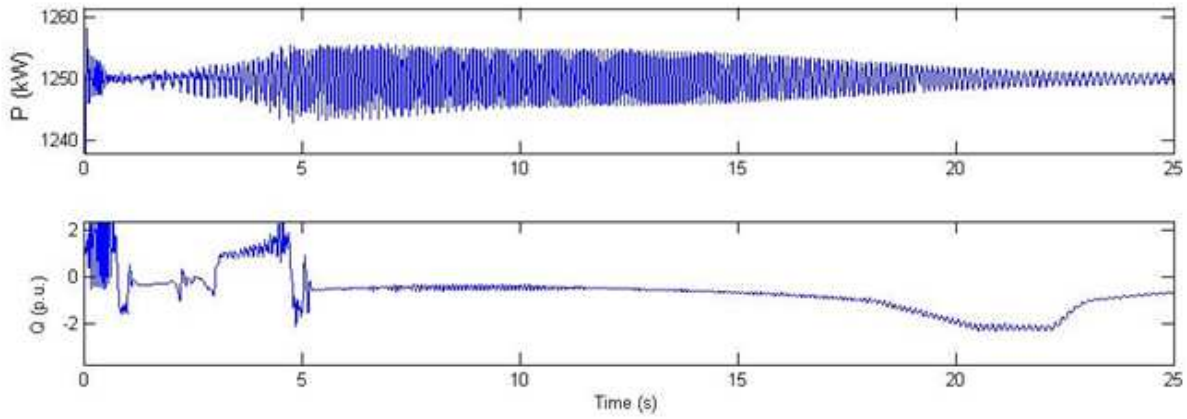

Fig. 4.10 Real Power Control for WTGS 2 (Challenges Pending with Independent Control)

Fig. 4.10 illustrates the changes in output real and reactive power for WTGS 2 while linearly varying wind speed and holding reactive power reference constant at 0 p.u. The output real power does not correlate with the changing wind speed even though the reactive power remains mostly constant. This challenge however prevents the independent control of real power.

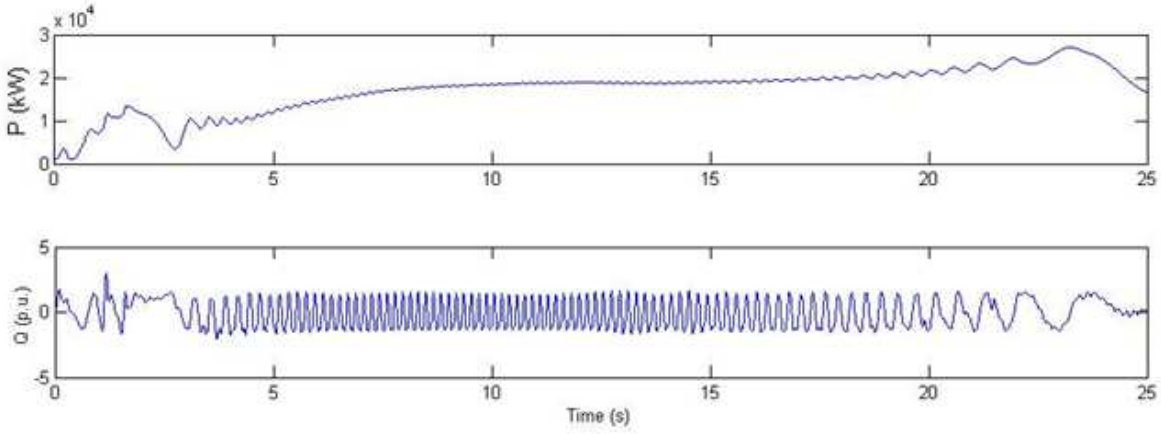

Fig. 4.11 Real Power Control for WTGS 3 (Challenges Pending with Independent Control)

Fig. 4.11 illustrates the changes in output real and reactive power for WTGS 3 while linearly varying wind speed and holding reactive power reference constant at 0 p.u. The output

real power changes with wind speed and corresponds to the power curve of the WG. Reactive power however oscillates between -1 p.u. and 1 p.u. making it challenging to independently control real power.

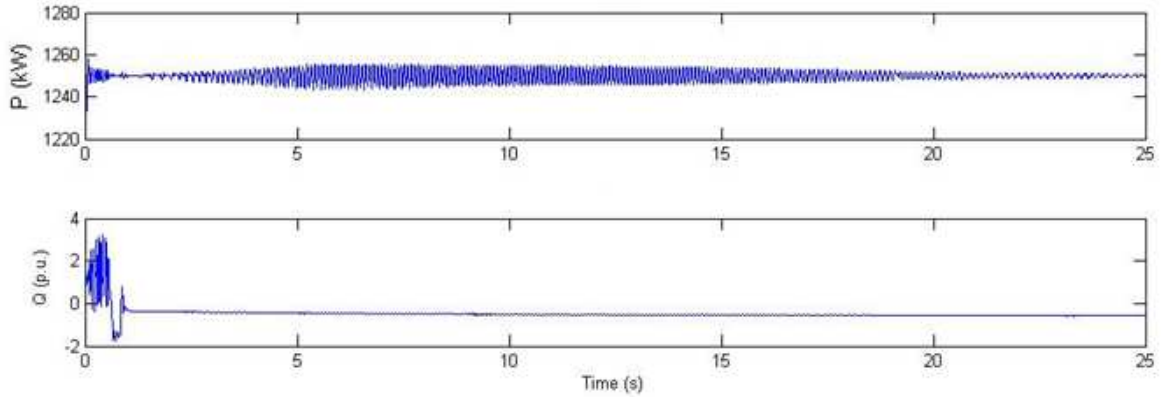

Fig. 4.12 Reactive Power Control for WTGS 4 (Challenges Pending with Independent Control)

Fig. 4.12 illustrates the changes in output real and reactive power for WTGS 4 while holding wind speed constant and changing reactive power reference from 0 p.u. to 0.5 p.u. Even though the real power oscillated about a 1.25 MW and stabilized, the reactive power output did not change with the change in the reference reactive power. Independent reactive power for this wind farm is therefore difficult.

Challenges Pending with Independent Control

Inability to attain independent real and reactive power control of the wind farms connected to the power grid was the major challenge observed among all four wind farms. One possible cause of these challenges could be as a result of inability in the rotor/grid side converter control. This is a subject for future study.

CHAPTER V

CONCLUSION

Objective of the Study

The objective of this study was to develop a platform for real-time simulation studies of Doubly-Fed Induction Generator (DFIG) based wind turbines integrated into large power systems. In addition, tests were done on the performance of two DFIG models on the platform real-time simulation model.

The real-time behavior of wind power system models were studied while connected to a large high voltage transmission network by developing a real-time power system model as a basis to study the real-time performance of grid connected wind power systems. The required tools and techniques needed to perform real-time simulation of wind power systems have been discussed. Also some of the challenges such as system size, and scalability of the models have been identified and discussed.

Summary of Findings and Conclusion

A platform model was real-time simulation model for DFIG based wind turbines was developed and used to test the performance of two DFIG models. Performance testing of grid-connected wind farms is essential in any research into the impact of wind farms on the power grid. In this study, the author investigated the behavior of two wind turbine models when

integrated into very large power networks. The main challenge was maintaining the stability of the model and the system, particularly in the case of the detailed wind power system.

The average model was found to be more stable than the detailed model for the large power system used in this study. It is recommended that a more robust DFIG model be designed to handle the case of integration into large scale power systems, since both models had an unstable reactive power converter.

REFERENCES

[1] L. Holdsworth, X. G. Wu, J. B. Ekanayake and N. Jenkins, "Comparison of fixed speed and doubly-fed induction wind turbines during power system disturbances," *IEE Proc. Generation, Transmission and Distribution,* vol. 150, no. 3, p. 343–352, 2003.

[2] T. M. Masaud and P. K. Sen, "Modeling and Control of Doubly fed Induction Generator for Wind Power," in *North American Power Symposium (NAPS),* 2011.

[3] G. Byeon, I. K. Park and G. Jang, "Modeling and Control of a Doubly-Fed Induction Generator (DFIG) Wind Power Generation System for Real-time Simulations," *Journal of Electrical Engineering & Technology,* vol. 5, pp. 61- 69, 2010.

[4] F. Wu, X.-P. Zhang, K. Godfrey and P. Ju, "Modeling and Control of Wind Turbine with Doubly Fed Induction Generator," in *IEEE PES Power Systems Conference and Exposition (PSCE),* 2006.

[5] M. Marinelli, A. Morini, A. Pitto and F. Silvestro, "Modeling of double fed induction generator (DFIG) equipped wind turbine for dynamic studies," in *43rd International Universities Power Engineering Conference (UPEC),* September 1-4, 2008.

[6] A. Junyent-Ferré, O. Gomis-Bellmunt, A. Sumper, M. Sala and M. Mata, "Modeling and control of the double fed induction generator wind turbine," *Simulation Modelling Practice and Theory,* vol. 18, pp. 1365-1381, 2010.

[7] A. P. Tennakoon, A. Arulampalam, J. B. Ekanayake and S. G. Abeyratne, "Modeling and Control of Doubly Fed Induction Generators (DFIGs) For Wind Energy Applications," in *First International Conference on Industrial and Information Systems, ICIIS,* Sri Lanka, 8 - 11 August 2006.

[8] H. Li, Z. Chen and J. K. Pedersen, "Optimal Power Control Strategy of Maximizing Wind Energy Tracking and Conversion for VSCF Doubly Fed Induction Generator System," in *CES/IEEE 5th International Power Electronics and Motion Control Conference (IPEMC),* 2006.

[9] P. B. Eriksen, T. Ackermann, H. Abildgaard, P. Smith, W. Winter and J. M. R. Garcia, "System operation with high wind penetration," *IEEE Power & Energy Magazine*, vol. 3, pp. 65-74, Nov. 2005.

[10] S. Muller, M. Deicke, and R. W. D. Doncker, "Doubly fed induction generator systems for wind turbine," *Industry Applications Magazine*, vol. 8, no. 3, p. 26–33, 2002.

[11] A. Petersson, Analysis, Modeling and Control of Doubly-Fed Induction Generators for Wind Turbines, in Energy and Environment, Goteborg: Chalmers University of Technology, 2010.

[12] M. Singh and S. Santoso, "Dynamic Models for Wind Turbines and Wind Power Plants," NREL, 2011.

[13] R. Datta and R. T. Ranganathan, "A method of tracking the peak power points for a variable speed wind energy conversion system," *IEEE Trans. Energy Conv.*, vol. 18, no. 1, pp. 163-168, 2008.

[14] A. G. Abo-Khail, D.-c. Lee and J.-K. Seok, "Variable speed wind power generation system based on fuzzy logic control for maximum output power tracking," in *35th Annual IEEE Power Electronics Specialists Conference*, Germany, 2004.

[15] R. Esmaili, L. Xu and D. K. Nichols, "A new control method of permanent magnet generator for maximum power tracking in wind turbine application," in *IEEE Power Engineering Society General Meeting*, June 12-16, 2005.

[16] B. Rabelo and W. Hofmann, "Control of an optimized power flow in wind power plants with doubly-fed induction generators," *IEEE 34th Annual Power Electronics Specialist Conference (PSEC)*, vol. 4, pp. 1563-1568, 2003.

[17] E. Muljadi and A. Ellis, "Validation of wind power plant models," in *IEEE Power and Energy Society General Meeting-Conversion and Delivery of Electrical Energy in the 21st Century*, 2008.

[18] M. Behnke, A. Ellis, Y. Kazachkov, T. McCoy, E. Muljadi, W. Price and J. Sanchez-Gasca, "Development and Validation of WECC variable speed wind turbine dynamic models for grid integration studies," in *AWEA Wind Power Conference*, 2007.

[19] T. Ackmann, Wind Power in Power Systems, John Wiley & Sons Ltd, 2005.

[20] The Mathworks, Inc., "Wind Farm - DFIG Detailed Model," [Online]. Available:

http://www.mathworks.com/products/simpower/examples.html?file=/products/demos/shipping/powersys/power_wind_dfig_det.html. [Accessed 10 March 2013].

[21] S. K. Salman and B. Badrzadeh, "New Approach for modelling Doubly-Fed Induction Generator (DFIG) for grid-connection studies," in *European Wind Energy Conference & Exhibition 2004*, 2004.

[22] L. Fan and S. Yuvarajan, "Modeling and Slip Control of a Doubley Fed Induction Wind Turbine Generator," in *North AmericanPower Symposium (NAPS)*, 28-30 Sept. 2008.

[23] P. Kundur, Power System Stability and Control, McGraw-Hill, 1994.

[24] D. W. Novotny and A. Lipo, Vector Control and Dynamics of AC Drives, Clarendon Press, 1996.

[25] R. Pena, J. C. Clare and G. M. Asher, "Doubly fed induction generator using back-to-back PWM converters and its application to variable-speed wind energy generation," *IEEE Proceedings on Electrical Power Applications*, vol. 143, no. 3, pp. 231-241, 1996.

[26] V. Erlich, J. Kretschmann, J. Fortmann, S. Mueller-Engelhardt and H. Wrede, "Modeling of wind turbines based on doubly-fed induction generators for power system stability studies," *IEEE Transactions on Power Systems*, vol. 22, no. 3, p. 909–919, 2007.

[27] K. Protsenko, B. Badrzadeh, P. F. Mayer and Z. Luo, "Application of Real Time Digital Simulation in Modeling Wind Turbines with Reduced and Full Converter Schemes".

[28] Opal-RT Technologies, Inc, "OP5600 off-the-shelf Hardware-in-the-Loop (HIL) simulator," 2012. [Online]. Available: http://www.opal-rt.com/product/op5600-hil-hardware-in-the-loop-computer-and-IO-system. [Accessed 5 March 2012].

[29] Opal-RT Technologies, Inc, "ARTEMiS," 2012. [Online]. [Accessed 6 March 2013].

[30] The MathWorks, Inc., "SimPowerSystems Videos & Examples," [Online]. Available: http://www.mathworks.com/products/simpower/examples.html. [Accessed 22 March 2013].

VITA

Nasir Abdulai Boakye-Boateng was born in Ijebu-Ode, Ogun State Nigeria, on December 28, 1984, eighth child to Ahmed Kwame Boakye and Haleema Agyekumwaa Boakye, both natives of Apaah in the Ashanti Region of Ghana. He completed Labone Senior High School in Accra, Ghana in December of 2000. In June of 2006 he completed his Bachelor of Science in Electrical and Electronic Engineering with Kwame Nkrumah University of Science and Technology, Kumasi, Ghana and then his Commonwealth Executive Master of Business Administration with the same institution in August of 2012. He was certified a Project Management Professional (PMP) in June of 2009 by the Project Management Institute. From 2006 to 2011 he served in various capacities with the Volta Aluminium Company Limited, Axon Information Systems, and MTN all in Ghana. In August 2011, he enrolled in the MS Electrical Engineering program at the University of Tennessee at Chattanooga. He is married with one daughter.

Permanent Address: 2627 Hixson Pike Apt 207
Chattanooga, Tennessee 37415
(973) 412-5267

This thesis was typed by the author.